Ingenieur-Archiv 59 (1989) 237—244

Ingenieur-Archiv

Computation of collapse loads in geomechanics by finite elements*

D. V. Griffiths, Manchester

Summary: Recent interest in bifurcation and localisation in geomechanics has led to a re-examination of traditional collapse calculations using finite element methods. This paper reviews some of the important aspects of calculations of this type from a practical viewpoint. Examples of collapse predictions in applications of both bearing capacity and slope stability with strain softening are presented. It is shown that localised zones of shear deformation can be modelled without any artificial inducements such as weak elements or applied displacement fields.

Berechnung von Einsturzlasten in der Bodenmechanik mit finiten Elementen

Übersicht: Das neuerliche Interesse an Verzweigung und Lokalisierung in der Bodenmechanik hat zu einer Überprüfung traditioneller Kollaps-Berechnungen nach der Finite-Element-Methode geführt. Hier werden vom praktischen Standpunkt einige wichtige Aspekte dieser Berechnungsmethode besprochen. Beispiele zur Versagensvorhersage bei der Tragfähigkeit und Hangstabilität von entfestigendem Material werden vorgestellt. Es wird gezeigt, daß lokalisierte Scherverformungen ohne Kunstgriffe mit nachgiebigeren Elementen oder erzwungenen Verschiebungsfeldern modelliert werden können.

1 Introduction

Computation of collapse loads in geomechanics using numerical analysis has received considerable attention in the literature over the past few years. Although it is not the intention of the present paper to give a historical review, considerable contributions were made by the Swansea school (e.g. [1—3]) during this period in developing robust implicit algorithms such as initial stress and viscoplasticity. Early initial stress calculations were also being performed by workers at Manchester (e.g. [4, 5]) and the viscoplastic formulation was later extended to cover a wide range of problems of geotechnical interest by Griffiths [6—8].

Recent interest in bifurcation and localisation in geomechanics has brought renewed interest in collapse calculations, particularly those in which some perturbation triggers the failure mechanism. Two types of perturbation can be distinguished; firstly due to meterial properties, where a softening stress/strain curve or a weak element is introduced [9, 10], and secondly due to geometric effects such as mesh design (e.g. [11]) or the introduction of a displacement field corresponding to a mode shape (e.g. [12]). One point that is not often emphasised, is that elastic-perfectly plastic materials also localise at failure. Indeed, any failure mechanism within a continuous body exhibits localisation between the failing material and surrounding material that still has reserves of strength. A well refined finite element mesh will be required to capture the zone of localisation, but a finite element mesh will always be limited in its ability to model large relative movements, especially in the context of small deformations.

---

* Presented at the workshop on Limit Analysis and Bifurcation Theory, held at the University of Karlsruhe (FRG), February 22—25, 1988

Rather surprisingly, the accurate computation of collapse loads does not require such mesh refinement. It has been shown many times that crude meshes are able to give good estimates of collapse loads without accurately modelling the shearing zone.

The remainder of this paper discusses some of the important features of collapse calculations using finite element methods from a practical viewpoint. Included in the discussion are comments concerning the correct choice of failure criterion, together with the best choice of element and algorithm. Examples of bearing capacity and slope stability are also presented.

2 Failure criteria

2.1 *Undrained clay*

Undrained clay represents an extreme of soil behaviour whereby strength is not a function of confining pressure. The most unambiguous failure criterion for this type of material is due to Tresca:

$$|\sigma_1 - \sigma_3| \leqq 2c_u \tag{1}$$

where c_u is the undrained cohesion and the principal stress σ_2 lies between σ_1 and σ_3. A more popular function is the von Mises criterion, but this can lead to ambiguity in the definition of c_u. For example, under triaxial conditions ($\sigma_2 = \sigma_3$) the criterion becomes

$$\sqrt{J_2} \leqq 2c_u/\sqrt{3} \tag{2}$$

whereas in plane strain (at failure: $\sigma_{2f} = (\sigma_1 + \sigma_3)/2$) the criterion becomes

$$\sqrt{J_2} \leqq c_u \tag{3}$$

where J_2 is the second deviatoric stress invariant. Referring to (2) and (3), c_u is the undrained cohesion measured under triaxial and plane strain conditions, respectively.

2.2 *Cohesionless soil*

The other extreme of soil behaviour is described by cohesionless soils which are wholly dependent on confining pressure for their strength. The best known criterion is due to Mohr-Coulomb which leads to an irregular hexagonal pyramid in principal stress space. Conical circular approximations to this surface are completely unsuitable (e.g. [13, 14]), but more complex smoothing functions such as those by Lade and Duncan [15] and Matsuoka and Nakai [16] have certain advantages for computational work. These surface both lie outside the Mohr-Coulomb pyramid and are based on experimental evidence in which full account is taken of the influence of σ_2. A typical quadrant of (dimensionless) principal stress space is shown in Fig. 1 for the case of $\varphi_c' = 30°$, where φ_c' is the friction angle measured in triaxial compression. The three criteria are

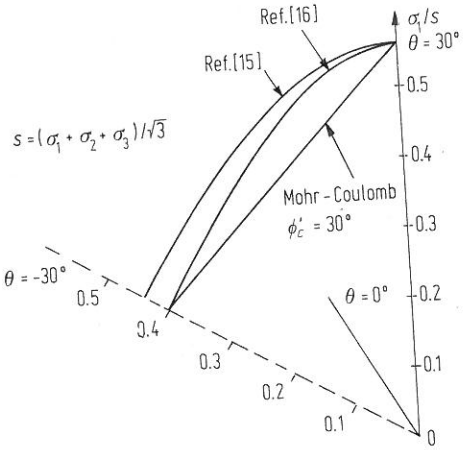

Fig. 1. Failure criteria for cohesionless soils in the deviatoric plane (θ: Lode angle)

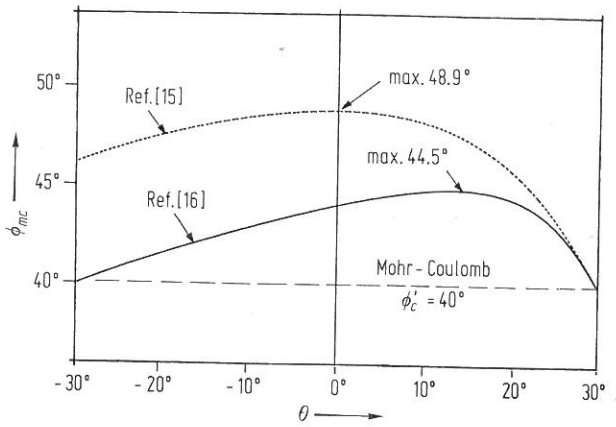

Fig. 2. Equivalent friction angle as a function of Lode angle

defined

$$\frac{\sigma_1}{\sigma_3} \leqq \tan^2(45° + \varphi_c'/2) \quad \text{(Mohr-Coulomb)}, \tag{4}$$

$$\frac{I_1 I_2}{I_3} \leqq \frac{9 - \sin^2\varphi_c'}{1 - \sin^2\varphi_c'} \quad \text{(Matsuoka-Nakai)}, \tag{5}$$

$$\frac{I_1^3}{I_3} \leqq \frac{(3 - \sin\varphi_c')^3}{(1 + \sin\varphi_c')(1 - \sin\varphi_c')^2} \quad \text{(Lade)} \tag{6}$$

where I_1, I_2 and I_3 are stress invariants. Even though these criteria are based on carefully conducted true triaxial tests, they differ by several degrees for certain stress paths. Figure 2 shows the friction angle implied by the two surfaces when fitted to Mohr-Coulomb at $\varphi_c' = 40°$ as a function of the Lode angle θ. All surfaces coincide in triaxial compression as expected, but for different values of the Lode angle the differences between the criteria become clear. For example, the Matsuoka-Nakai surface gives the same friction angle in extension and compression whereas Lade's surface indicates a triaxial extension friction angle some 6° higher. Under plane strain conditions where $\theta \approx 20°$, both criteria give friction angles approximately 5° higher than in triaxial compression. This latter observation is well supported by experimental evidence, although the difference observed in triaxial extension is more open to debate due to possible inherent instabilities caused by specimen necking.

In summary, even the most carefully derived failure criteria differ by several degrees for certain stress paths. This reflects the current state of knowledge and the level of confidence with which the friction angle can be measured in the laboratory.

3 Element type

The majority of publications in which collapse loads are predicted using finite element analyses have used the 8-node quadrilateral element with reduced (2 by 2) integration. This element and integration level have been shown to be reliable for both plane and axisymmetric strain applications. The element has been criticised however on the grounds that reduced integration is necessary in order to relax the volumetric constraints imposed by different plastic flow rules. If using exact integration, higher order elements such as the 15-noded, cubic strain triangle have been suggested [17] as suitable for collapse predictions, especially in axisymmetry. For this element in plane strain, 12 integration points are required whereas in axisymmetry, 16 points are recommended. It should be noted however, that due to terms like $1/r$ in the strain-displacement relationships, exact integration of the stiffness matrix in axisymmetry is impossible using conventional quadrature rules.

In spite of its added complexity, the 15-noded triangle is easily incorporated into finite element software that is suitable modular [18]. When using the 15-noded triangle, far fewer elements will be necessary than a corresponding analysis with the same number of degrees of freedom using a lower order element such as the 9-noded quadrilateral. The bandwidths will be correspondingly higher however, typically leading to twice as much storage requirement.

Future developments may well be away from high order elements towards even lower order elements such as the 4-noded quadrilateral. This approach requires a computational gimmick called selective reduced integration (e.g. [19]) and has been shown to be quite effective for some collapse calculations [20]. Further testing of this element and integration scheme will be necessary however, before any conclusive recommendations can be made about its effectiveness.

4 Algorithms for stress redistribution

Much discussion has recently centred around the best numerical method for redistributing stresses that have strayed into illegal stress space outside the failure surface. Two main types of algorithm have emerged which tackle this problem either locally or globally.

The global approach arranges for stresses to return to the failure surface in an average sense only. Initial stress and viscoplastic algorithms are of this type, and the simplest approaches use modified Newton-Raphson iterations with the global stiffness matrix formed once only. No attention is paid to the route by which individual stress points return to the failure surface once they have strayed outside. Clearly, the saving in computer time enjoyed from only having to operate on one global stiffness matrix is offset by added iterations as failure is approached. Variations on this theme are of course possible, whereby the global (tangent) stiffness matrix is reformed occasionally to meet some efficiency compromise.

The local approach attends in some detail to the means by which individual stress points return to the failure surface. Various algorithms have been proposed for integration of the plastic rate equations, some of which are explicit while others require iterations at the local level. A review of some of the alternatives has been summarised by Ortiz and Popov [21].

It would seem that many different methods are available for computation of collapse loads in geomechanics. Unfortunately, research workers in this area rarely publish their code, so one can only speculate as to how some of the trickier algorithmic details are dealt with. Until objective comparisons between software from different sources are made, progress towards more accurate and efficient algorithms will be hindered. In addition, there is a danger that some individual approaches for the computation of collapse loads may lead to conclusions which say more about the algorithm used than the physics of the problem.

In the next section, two problems of collapse in geomechanics are presented. In both cases, a simple viscoplastic global algorithm is used with a full modified Newton-Raphson iterative scheme. The software is published in full in the text by Smith and Griffiths [18].

5 Analysis of bearing capacity

The example is of a rigid, smooth strip footing on an elastic-perfectly plastic, weightless soil governed by the Mohr-Coulomb failure criterion. The footing is 4 m wide, but due to symmetry only half the problem is analysed. The elastic soil parameters are $E = 10^5$ kPa, $\nu = 0.3$ with shear strength values, $\varphi' = 40°$, $c' = 1$ kPa. The dilation angle is put to zero, indicating a non-associated flow rule with no plastic volume change. This problem was chosen because the combination of a high friction angle and low dilation angle was considered quite a severe test of the algorithm. An unsuccessful attempt to solve the same problem was made by de Borst and Vermeer [22], leading those authors to make rather general conclusions that were really only applicable to their particular solution method.

In the present analysis, increments of prescribed displacements equal to 0.25 mm were applied to the footing in the vertical direction. The mesh used to solve the problem is shown in

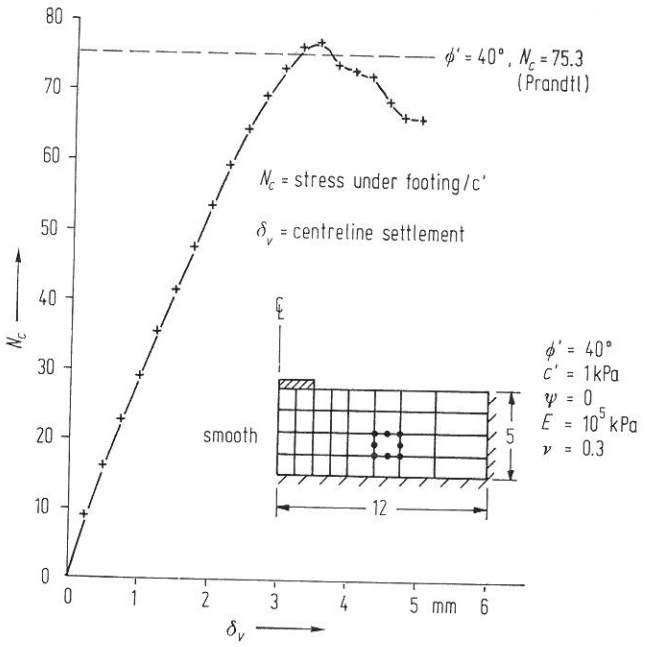

Fig. 3. Bearing capacity of a weightless soil with $\varphi' - \psi = 40°$ (ψ: dilatancy angle)

Fig. 3, together with a plot of the mobilised bearing capacity factor N_c vs. footing displacement. A smooth curve is obtained prior to failure, which takes place very close to the analytical solution of Prandtl ($N_c = 75.3$). Beyond the peak, the curve becomes unstable due to numerical softening; a phenomenon also observed in some of the results obtained in [22].

6 Analysis of slope stability

The second example involves the analysis of a slope of undrained clay in plane strain under gravity loading. A von-Mises failure criterion of the type given by (3) was used, incorporating a softening stress strain curve of the type shown in Fig. 4. The material was assumed to remain elastic until a peak strength given by cohesion c_p was reached. Beyond the peak strain, the material weakens at a rate governed by the gradient H of the softening limb of the curve. In the present work, the stress/strain behaviour is defined in terms of the following invariants of stress and strain:

$$\bar{\sigma} = \frac{1}{\sqrt{2}} \sqrt{(\sigma_{xx} - \sigma_{yy})^2 + (\sigma_{yy} - \sigma_{zz})^2 + (\sigma_{zz} - \sigma_{xx})^2 + 6\sigma_{xy}^2}, \tag{7}$$

$$\bar{\varepsilon} = \frac{\sqrt{2}}{3} \sqrt{(\varepsilon_{xx} - \varepsilon_{yy})^2 + (\varepsilon_{yy} - \varepsilon_{zz})^2 + (\varepsilon_{zz} - \varepsilon_{xx})^2 + \frac{3}{2}\varepsilon_{xy}^2} \tag{8}$$

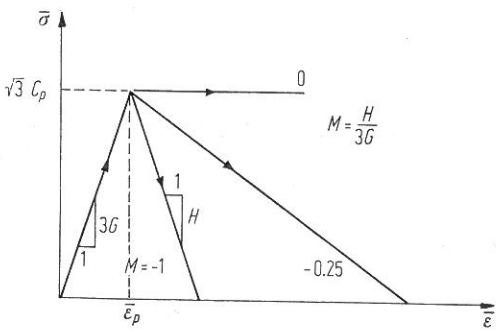

Fig. 4. Typical stress/strain curves for softening model

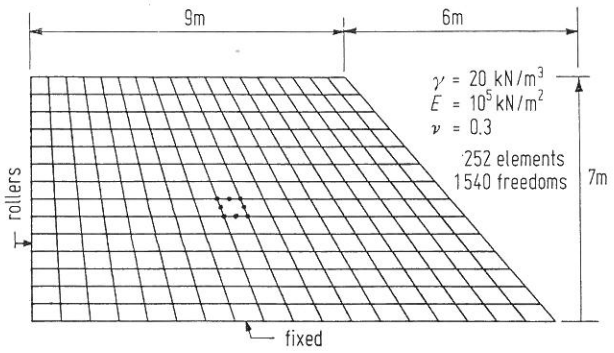

Fig. 5. Mesh used for slope stability analyses

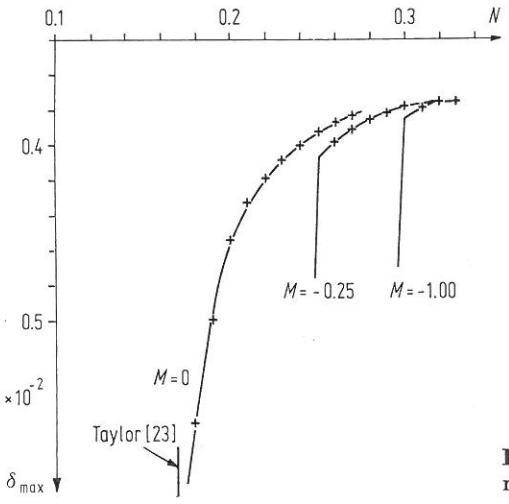

Fig. 6. Maximum displacement of slope vs. stability number

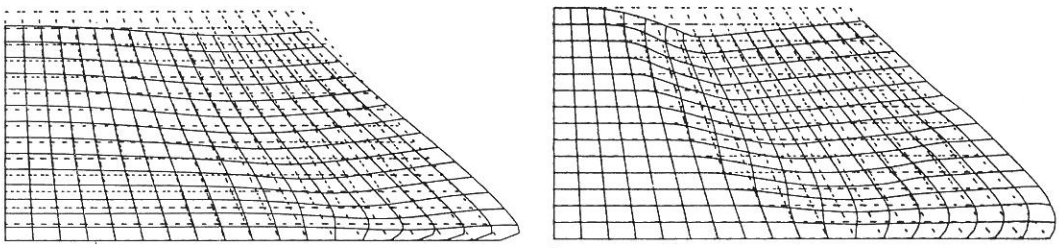

Fig. 7. Deformed mesh of slope at failure. **a** $M = 0$; **b** $M = -0.25$

where $\varepsilon_{zz} = 0$ in plane strain. With these definitions of stress and strain, the gradient of the elastic portion of the curve equals $3G$, where G is the elastic shear modulus. The degree of post-peak softening is therefore conveniently defined through a dimensionless brittleness coefficient M which is the ratio of the gradients post- and pre-peak, thus

$$M = H/(3G)\,. \tag{9}$$

At any stage of the analysis, the cohesion is computed according to the formulae

$$c = c_p \quad \text{if} \quad \bar{\varepsilon} \leqq \bar{\varepsilon}_p\,, \tag{10}$$

$$c = c_p + H(\bar{\varepsilon} - \bar{\varepsilon}_p)/\sqrt{3} \quad \text{if} \quad \bar{\varepsilon} > \bar{\varepsilon}_p \tag{11}$$

where

$$\bar{\varepsilon}_p = \sqrt{3}\, c_p/(3G)\,. \tag{12}$$

As shown in Fig. 4, the residual strength is assumed to equal zero, although a larger value could easily be introduced if required.

The problem to be analysed is a 7 m high slope inclined at just under 50° to the horizontal. The slope rests directly on a firm foundation as indicated by the mesh shown in Fig. 5 which has 1540 degrees of freedom. Gravity nodal loads were generated in the usual way by numerical integration of the shape functions assuming a total unit weight of 20 kN/m³. The gravity loads were applied to the initially unstressed slope in a single increment, and failure was generated by keeping M constant and gradually reducing the peak cohesive strength in the form of a stability number N, defined by

$$N = c_p/(\gamma H). \tag{13}$$

Failure was said to have occured when the algorithm failed to converge in 100 iterations with correspondingly large rates of increase of nodal displacements.

It was found that even a gentle softening of the stress/strain curve could result in a very sudden failure of the slope when a critical value of N was reached. This might be expected in a load controlled environment once some of the Gauss points start to soften. The stress redistribution following softening of one or two Gauss points would throw a considerable burden of shear stress on neighbouring points, which in their turn would soften, and so on. As indicated by the graphs of N vs. maximum displacement δ_{max} in Fig. 6, the softening slopes transformed quickly from an entirely elastic condition to complete collapse. For the elastic-perfectly plastic case ($M = 0$), a more gentle curve was observed but close agreement was still achieved with Taylor's [23] solution.

The deformed mesh at failure for two values of M is shown in Fig. 7. Before plotting the figures, the elastic displacements due to gravity loading were subtracted from the total displacements (after 100 iterations) to leave the plastic displacements. The displacements at failure for the case of $M = 0$ (i.e. perfect plasticity) are given in Fig. 7a, and a rather diffuse mechanism is apparent with the entire mesh moving down and to the right. The displacements at failure for the case of $M = -0.25$ (Fig. 7b), clearly demonstrate the concentration of shear deformations along a quite narrow shear band following an approximately circular path. A finer mesh would lead to a further narrowing of the shear band, and, depending on the degree of refinement, would also tend to increase slightly the value of N to cause failure of the softening slope.

Further numerical studies on the behaviour of softening soils are currently being performed at Manchester University by the author and others (e.g. [24]). These studies will be reported more fully at a later date.

7 Conclusions

The paper has reviewed some important considerations in the computation of collapse loads in geomechanics using finite element methods. The importance of the choice of failure criterion, especially for cohesionless soils was emphasised. Two failure criteria based on carefully performed triaxial tests were examined, and a range of uncertainty of up to 6° for triaxial extension stress paths demonstrated.

Some popular element types for collapse calculations were reviewed, but the choice of element did not seem to be of prime concern provided the appropriate order of integration was used. From practical considerations however, simpler elements are more likely to prove popular with the non-specialist.

Numerical examples of bearing capacity and slope stability involving a strain softening material were presented using a simple Newton-Raphson iterative approach [18]. The bearing capacity exercise confirmed that a large difference between the friction and dilation angles should not be an obstacle to accurate collapse prediction using finite elements. The slope stability example with a softening stress/strain curve, demonstrated that localisation in the form of a zone of concentrated shear deformation can be modelled in certain problems without any triggering in the form of weak elements or the application of special displacement fields.

A considerable variety of algorithms for collapse calculations are used by different workers. Although usually leading to similar solutions, occasional discrepancies cause confusion and can lead to erroneous conclusions. In the future, greater interchange and publishing of software is to be encouraged. This should lead to significant algorithmic improvements as the best features from different methods are combined.

References

1. Zienkiewicz, O. C.; Valliappan, S.; King, I. P.: Elasto-plastic solution of engineering problems: Initial stress finite element approach. Int. J. Numer. Methods Eng. 1 (1969) 75—100
2. Zienkiewicz, O. C.; Humpheson, C.; Lewis, R. W.: Associated and non-associated plasticity and visco-plasticity in soil mechanics. Geotechnique 25 (1975) 671—689
3. Zienkiewicz, O. C.; Norris, V. A.; Winnicki, L. A.; Naylor, D. J.; Lewis, R. W.: A unified approach to the soil mechanics of offshore foundations. In: Zienkiewicz, O. C.; Lewis, R. W.; Stagg, K. G. (eds.) Numerical methods in offshore engineering, pp. 361—412. Chichester, New York: John Wiley and Son
4. Smith, I. M.: Numerical analysis of plasticity in soils. In: Palmer, A. C. (ed.) Symp. on plasticity and soil mechanics, Cambridge University, pp. 279—289. Cambridge: Cambridge Instant Print 1973
5. Smith, I. M.; Hobbs, R.: Finite element analysis of centrifuged and built-up slopes. Geotechnique 24 (1974) 531—559
6. Griffiths, D. V.: Finite element analyses of walls footings and slopes. In: Randolph, M. F. (ed.) Symp. on computer applications to geotechnical problems in highway engineering. Cambridge, UK, pp. 122—146. Cambridge: P. M. Geotechnical Analysts Ltd. 1980
7. Griffiths, D. V.: Elasto-plastic analyses of deep foundations in cohesive soils. Int. J. Numer. Anal. Methods Geomech. 6 (1982) 211—218
8. Griffiths, D. V.: Computation of bearing capacity factors using finite elements. Geotechnique 32 (1982) 195—202
9. Griffiths, D. V.: Computation of strain softening behaviour. In: Desai, C. S.; Saxena, S. K. (eds.) Symp. on implementation of computer procedures and stress-strain laws in geotechnical engineering, pp. 591—603. Durham, North Carolina: Acorn Press 1981
10. Prevost, J. H.: Localisation and deformation in elastic-plastic solids Int. J. Numer. Anal. Methods Geomech. 8 (1984) 187—196
11. Hsu, T. S.; Peters, J. F.; Saxena, S. K.: Importance of mesh design for capturing strain localisation. In: Desai, C. S.; Krempl, E.; Kiousis, P. D.; Kundu, T. (eds.) Proc. 2nd Int. Conf. constitutive laws for eng. mat., pp. 857—864. New York: Elsevier 1987
12. de Borst, R.: Bifurcations in finite element models with a nonassociated flow rule. Int. J. Numer. Anal. Methods Geomech. 11 (1988) 99—116
13. Bishop, A. W.: The strength of soils as engineering materials (6th Rankine lecture). Geotechnique 16 (1966) 91—130
14. Griffiths, D. V.: Some theoretical observations on conical failure criteria in principal stress space. Int. J. Solids Struct. 22 (1986) 553—565
15. Lade, P. V.; Duncan, J. M.: Elasto-plastic stress-strain theory for cohesionless soils. Proc. ASCE GT 101 (1975) 1037—1053
16. Matsuoka, H.; Nakai, T.: Stress-deformation and strength characteristics of soil under three different principal stresses. Proc. JSCE 232 (1974) 59—70
17. Sloan, S. W.; Randolph, M. F.: Numerical prediction of collapse loads using finite element methods. Int. J. Numer. Anal. Methods Geomech. 6 (1982) 47—76
18. Smith, I. M.; Griffiths, D. V.: Programming the finite element method (2nd ed.) Chichester, New York: J. Wiley and Son 1988
19. Hughes, T. J. R.: The finite element method. Englewood Cliffs, New Jersey: Prentice-Hall, 1987
20. Prevost, J. H.; Hughes, T. J. R.: Finite element solution of elastic-plastic boundary value problems. ASME J. Appl. Mech. 48 (1981) 69—74
21. Ortiz, M.; Popov, E. P.: Accuracy and stability of integration algorithms for elasto-plastic constitutive relations. Int. J. Numer. Methods Eng. 21 (1985) 1561—1579
22. de Borst, R.; Vermeer, P. A.: Possibilities and limitations of finite elements for limit analysis. Geotechnique 34 (1984) 199—210
23. Taylor, D. W.: Stability of earth slopes. J. Boston Soc. Civ. Eng. 24 (1937) 197—246
24. Shuttle, D. A.; Smith, I. M.: Numerical simulation of shear band formation in soils. Int. J. Numer. Anal. Methods Geomech. 6 (1988)

Received May 6, 1988

Dr. D. V. Griffiths

Simon Engineering Laboratories
University of Manchester
Manchester M 13 9PL
UK